American Mineralogist, Volume 90, pages 1840–1851, 2005

Model pyroxenes III: Volume of *C*2/*c* pyroxenes at mantle *P*, *T*, and *x*

RICHARD M. THOMPSON,[1,*] ROBERT T. DOWNS,[1] AND GÜNTHER J. REDHAMMER[2]

[1]Department of Geosciences, University of Arizona, Tucson, Arizona 85721-0077, U.S.A.
[2]Institut für Kristallographie, Rheinisch Westfälische Technische Hochschule Aachen, Jägerstrasse 17/19, 54056 Aachen, Germany

ABSTRACT

Variations in unit-cell volumes of mantle minerals as functions of *P* and *T* are important parameters in the description of the interior of the Earth and the behavior of materials. Recently, Thompson and Downs (2004) presented a model for the crystal structures of pyroxenes parameterized in terms of the O3-O3-O3 angle, θ, and the oxygen radius, *r*. This model has proven useful in the analysis of compression and expansion mechanisms in pyroxenes, providing an understanding of θ and r as functions of *P* and *T*. However, it did not provide a basis for analyzing changes in some properties that are strongly dependent on composition.

In this paper, we show that ambient unit-cell volumes of the *C*2/*c* pyroxenes are correlated with M1 cation radius. This relationship can be used to calculate model ambient unit-cell volumes as a function of chemistry. From this starting point, pyroxene unit-cell volume variation with *P* and *T* can be modeled as a function of θ(*P*,*T*) and *r*(*P*,*T*). These relationships are investigated for diopside, hedenbergite, acmite, jadeite, and kosmochlor. The model reproduces observed unit-cell volumes of these phases recorded at *P* to within 0.09% and at *T* to within 0.10%, at simultaneous *P* and *T* for jadeite to within 0.57%, and at simultaneous *P* and *T* for diopside to within 1.20%. K_o and K' from third-order Birch-Murnaghan fits to the observed volume vs. pressure relationships and those calculated from the Thompson-Downs model are statistically the same. The fit of the Thompson-Downs EOS to the observed data is compared to the fit of the third order Birch-Murnaghan. The model is used to create an algorithm that estimates volumes for *C*2/*c* pyroxenes as a function of *P*, *T*, and *x*.

INTRODUCTION

An understanding of the behavior and properties of mantle materials at deep Earth pressures and temperatures is important for several reasons, including the geophysical and geochemical modeling of the earth and other planetary bodies (Mao and Hemley 1998). An important terrestrial example is the interpretation and analysis of seismic data. Direct observation of Earth materials at mantle conditions is extremely challenging. Much accepted understanding of the deep Earth results from the extrapolation of observations made at lower temperatures and/or pressures. This work can be extended by virtual investigations into the mantle using various kinds of models.

The term pyroxene refers to a group of minerals and synthetic materials with similar crystal structures that include important components of the Earth's crust and mantle, lunar and Martian rocks, and meteorites (Deer et al. 1978). Variations in the volumes of pyroxenes as functions of *P*, *T*, and *x* need to be understood to develop realistic mineralogical models of the upper mantle that are consistent with seismic profiles. Theoretical approaches to developing equations of state include quantum statistical techniques, lattice dynamics (cf. Duffy and Wang 1998), molecular dynamics simulations (cf. Matsui and Price 1992), and topological models with energy modeling (cf. Matsui and Busing 1984). In this paper, we apply the topological model of Thompson and Downs (2004) to the analysis of volume changes in *C*2/*c* pyroxenes with *P*, *T*, and *x*.

Many studies have utilized topological models of pyroxenes to analyze observed structures (cf. Thompson 2004). Thompson (1970) used physical models of regular octahedra and tetrahedra to derive rules governing the relationships between octahedral and tetrahedral chains in hypothetical idealized pyroxenes and to predict the most likely high-pressure polymorphs. Papike et al. (1973), building on the work of Thompson (1970), suggested explanations for the observed tetrahedral chain geometries in pyroxenes. Pannhorst (1979, 1981) presented model pyroxenes built from planar subunits and emphasized the role of M2-O3 bonding changes in transitions between the polymorphs. Chisholm (1981, 1982) built model pyroxenes from linear subunits, and proposed a rule for combining them that limited the number of possible polymorphs, but allowed the commonly occurring ones. Downs (2003) used analysis of procrystal electron densities to determine the bonding topologies of the pyroxenes and further established the relationship between M2-O3 bonding and symmetry. Hattori et al. (2000) derived the crystal structure of an ideal cubic closest-packed *C*2/*c* pyroxene to demonstrate that $FeGeO_3$ moves toward CCP with pressure. Thompson and Downs (2003) derived cell parameters and asymmetric units for the 81 possible ideal closest-packed pyroxenes based on stacking sequences of length 12 or less to find crystallographic parameters important in determining observed topologies. The last two studies provided the means for quantitative comparison

* E-mail: thompson@geo.arizona.edu

0003-004X/05/1112–1840$05.00/DOI: 10.2138/am.2005.1854

between the models and observed pyroxenes, but were limited by their static nature in their ability to model pyroxene behavior under changing conditions.

Thompson and Downs (2004) derived model pyroxenes with regular M1 and T polyhedra, and arbitrary tetrahedral chain geometry (hereafter referred to as the TD model). The TD model provides a means to calculate the crystal structure of a model pyroxene from two parameters: the O3-O3-O3 angle, θ, and the model oxygen radius, *r*. The parameter θ determines the tetrahedral chain geometry, while both *r* and θ affect the unit-cell volume. The M1 octahedral volume also varies with both θ and *r*. The volume vs. θ curves for both the M1 octahedron and the bulk structure resemble an inverted parabola with a volume maximum when θ = 180° and minima at 120 and 240°, the endpoints of the interval of physically meaningful values for θ. Varying *r* while leaving θ fixed results in an equivalent isotropic variation in the cell edges of the model crystal, so varying *r* is the model equivalent of isotropically compressing or expanding the crystal.

The TD model was designed to be simple and physically realistic. Real pyroxenes have M1 and T that are nearly regular, and structures within a given polytype differ mainly in their tetrahedral chain geometry and volume (Thompson and Downs 2004). The model requirement that M1 and T be regular polyhedra means that the geometry of a given model pyroxene is determined by the geometry of the tetrahedral chain, which can be characterized by the parameter θ. Other possible choices for a parameter describing tetrahedral chain geometry cannot be defined so as to provide a one-to-one relation between the parameter and every possible chain orientation. For example, the O3-T-O3 angle is the same when θ = 170 and 190°. The parameter θ has been a traditional choice for examination in the analysis of pyroxene behavior with changing *P*, *T*, and *x* (cf. Cameron et al. 1973; Papike et al. 1973, Zhang et al. 1997; Arlt and Angel 2000; Tribaudino et al. 2002). Combining θ with a volume scaling parameter such as *r* provides a logical basis for a realistic pyroxene model.

The TD model was designed primarily to analyze compression and expansion mechanisms by quantifying the effect of changes in the tetrahedral chain orientation on crystallographic parameters such as unit-cell volume, interatomic distances, and distortion from closest-packing. Comparison of model and observed structures demonstrates that tetrahedral rotation is an important mechanism for changes with *P* and *T* and allows quantification of the contribution of rotation to those changes. The model shows that tetrahedral rotation accounts for much of the compressional anisotropy in *C*2/*c* pyroxenes, which can be as high as 1:2.3:2.3 (diopside = Levien and Prewitt 1981).

The model provides insight into the variation of many properties with *x*, such as the structurally important M-T distances. It also provides an explanation for the different bonding topologies seen in pyroxenes. Finally, comparing the observed structures with model equivalents (same unit-cell volume, tetrahedral chain geometry) can give insight into the forces distorting the observed topologies from model arrangements.

However, the model does not explain the relationship between observed ambient condition unit-cell volumes and θ as chemistry varies. Raudsepp et al. (1990b) reported the approximate linearity of monoclinic pyroxene cell-dimensions with variation in M1 cation radius. Redhammer et al. (2003) concluded that the size of the M1 cation radius was the controlling factor in the variation of many structural parameters with chemistry in the sodium pyroxenes and in the low-temperature behavior of $NaTiSi_2O_6$. Redhammer and Roth (2004) reached the same conclusion about the variation with chemistry of many structural parameters, including unit-cell volume, in the $LiMSi_2O_6$ pyroxenes. In the current work, the relationship between M1 cation radius and unit-cell volume is investigated, and combined with the TD model. A modification of the TD model is developed that reproduces important compressional properties of the sodium and calcium clinopyroxenes. The model is used to predict the volumes of these pyroxenes at simultaneous *P* and *T*.

VOLUME VARIATION WITH COMPOSITION

We have examined the relationship between ambient condition unit-cell volume and M1 cation radius (Shannon 1976) for 22 *C*2/*c* end-member silicate pyroxene crystal structures taken from the literature. Table 1 contains relevant data and references for these pyroxenes. The relationship between unit-cell volume and M1 cation radius for these pyroxenes is illustrated in Figure 1. The data are separated into four subsets, each with fixed M2 chemistry (Li, Na, Ca, and Zn) to facilitate comparison of the effects of M1 cation radius on unit-cell volume with the effects of M2 cation radius. The M1 cation radii for the 22 pyroxenes display a linear correlation with unit-cell volume ($R^2 = 0.92$). The linear correlations within each of the four subsets with fixed M2 have higher R^2 (0.96 to 0.98).

The effect of changes in M2 radius on unit-cell volume can be

TABLE 1. Unit-cell volumes, M1-cation radii (Shannon 1976), and O3-O3-O3 angles for *C*2/*c* silicate pyroxenes at ambient conditions

M2M1	*V* (Å^3)	*r*(M1) (Å)	∠O3-O3-O3 (°)	Reference
LiAl	388.79	0.535	189.9	Arlt and Angel (2000)
LiV	413.08	0.640	181.9	Satto et al. (1997)
LiFe	415.95	0.645	180.8	Redhammer et al. (2001)
LiTi	423.93	0.67	180.7	Kopnin et al. (2003)
LiGa	405.05	0.620	179.9	Sato et al. (1994)
LiSc	440.83	0.745	175.6	Hawthorne and Grundy (1977)
LiIn	447.77	0.800	167.4	Redhammer and Roth (2004)
NaAl	402.03	0.535	174.7	Downs and Thompson (in prep)
NaMn	423.85	0.645	174.1	Ohashi et al. (1987)
NaFe	428.69	0.645	174.1	Downs et al. (in prep)
NaTi	436.35	0.67	173.9	Ohashi et al. (1982)*
NaSc	455.20	0.745	173.7	Ohashi et al. (1994a)
NaV	426.72	0.640	173.0	Ohashi et al. (1994b)
NaCr	418.85	0.615	172.8	Origlieri et al. (2003)
NaGa	417.73	0.62	172.7	Ohashi et al. (1995)
NaIn	463.38	0.800	171.1	Ohashi et al. (1990)
CaMg	438.63	0.720	166.5	Downs and Thompson (in prep)
CaNi	435.21	0.69	165.2	Ghose et al. (1987)
CaCo	443.52	0.75	165.1	Ghose et al. (1987)
CaFe	449.89	0.780	164.4	Zhang (1997)
CaMn	466.02	0.83	163.8	Freed and Peacor (1967)
ZnZn	442.10	0.74	161.3	Morimoto et al. (1975)

Notes: M2 radii are *r*(Li) = 0.76 Å, *r*(Na) = 1.02 Å, *r*(Ca) = 1.12 Å, and *r*(^{IV}Zn) = 0.60 Å.

* These crystals have reexamined twice since the original structure determination: fourteen years later by Ohashi et al. (2003c) as part of the $NaTiSi_2O_6$-$CaMgSi_2O_6$ solid solution series (V = 438.84 Å^3) and 23 years later by Redhammer et al. (2003) as part of a low-temperature study that revealed the *C*2/*c*-*P*$\bar{1}$ phase transition ($V_{298\,K}$ = 437.77).

illustrated by looking along an imaginary vertical line in Figure 1 that intercepts at 0.75 Å. The M1 radius can be considered fixed for the four pyroxenes in the M1 radius domain (0.74–0.75Å), allowing analysis of the effects of M2 radius on cell size. The radius of M2 ranges from 0.60 to 1.12 Å over this domain, while the unit-cell volume varies by 14 Å^3, or about 3%. In addition, a plot of volume vs. M2 radius for these four pyroxenes (Fig. 2) demonstrates that these quantities are not linearly correlated.

By way of contrast, we can investigate the effects of M1 radius on unit-cell volume by examining a collection of pyroxenes with identical M2 chemistry. For instance, nine of the pyroxenes in Figure 1 have sodium at the M2 site, and are represented by solid circles. Across the sodium pyroxenes, the M1 radius varies from 0.535 to 0.80 Å (half as much as M2 varied in the previous example), while the unit-cell volume changes by 61 Å^3 (vs. 14 Å^3 across the larger M2 domain in the previous example). The relationship between M1 radius and volume is linear for the sodium pyroxenes (R^2 = 0.98), as it is for each of the series of ambient-condition pyroxenes (Fig. 1). Our interpretation is that the M1 chains of nearly regular, edge-sharing octahedra form a rigid scaffold, the size of which has the most significant influence on unit-cell volume.

Variation in the geometry of the flexible tetrahedral chains of the pyroxenes is commonly characterized using the size of the O3-O3-O3 angle, θ. The variation of θ with unit-cell volume is illustrated in Figure 3 for the 22 ambient-condition pyroxenes listed in Table 1, as well as for diopside and kosmochlor at elevated temperatures and pressures (diopside = Downs and Thompson, in prep; Cameron et al. 1973; kosmochlor = Origlieri et al. 2003; Cameron et al. 1973). On one hand, the variation of θ with unit-cell volume for the end-member ambient condition pyroxenes of various chemistries, denoted by the solid squares, has a poorly defined negative trend that correlates small θ values with large unit-cell volumes and large θ values with smaller volumes. On the other hand, data for pyroxenes of fixed composition recorded at non-ambient conditions (hollow symbols) display well-defined positive trends with small θ values associated with small unit-cell volumes and larger θ values associated with larger volumes. Also shown in Figure 3 is a line representing the model variation of θ with unit-cell volume when assuming perfectly regular M1 octahedra and flexible tetrahedral chains of perfectly regular tetrahedra (Thompson and Downs 2004) and fixed model oxygen radius, r = 4/3 Å. This line has symmetrical regions of positive and negative correlation between volume and θ, mirroring each other about the volume maximum at θ = 180°, the value at which the tetrahedral chains are fully extended. We will show later that by varying the model oxygen radius, r, in systematic combination with tetrahedral rotation (i.e., varying θ), we can reproduce observed unit-cell volumes at P and T.

Mixing volume variation with M1 composition

The dependence of unit-cell volume on M1 chemistry in end-member pyroxenes (Fig. 1) suggests that mixing volumes in pyroxenes with variable and completely disordered M1 chemistry may be largely determined by the M1 site. Mixing volume for a solid solution of two end-members, e_1 and e_2, is defined by: $V_{mix} = V_{observed} - (Xe_1Ve_1 + Xe_2Ve_2)$, where Xe_i is the mole fraction of the end-member, e_i, in the solution. A simple possibility is that

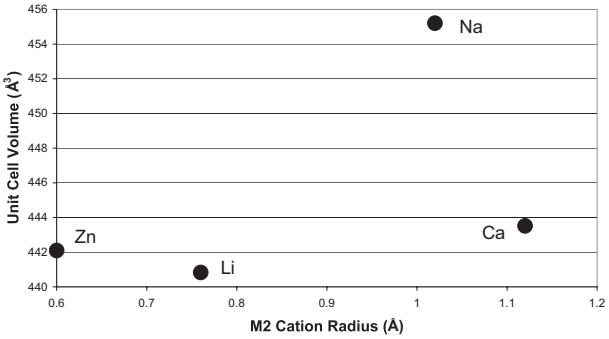

FIGURE 2. A plot illustrating the asystematic relationship between unit-cell volume and M2 cation radius (Shannon 1976) for four ambient condition $C2/c$ pyroxenes ($ZnSiO_3$, $LiScSi_2O_3$, $NaScSi_2O_3$, and $CaCoSi_2O_3$ references are in Table 1) that have nearly equal M1 radius (between 0.74 Å and 0.75 Å).

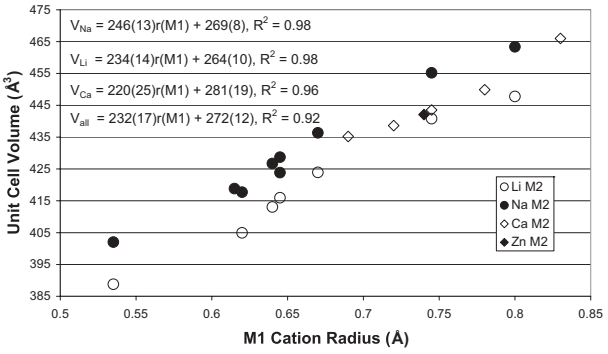

FIGURE 1. The correlation between unit-cell volume and M1 cation radius (Shannon 1976) for 22 ambient condition $C2/c$ pyroxenes taken from the literature. Pyroxene references are in Table 1. Equations are derived from linear least-square fits to the unit-cell volumes of four pyroxene series, where each series has fixed M2 chemistry, denoted by the subscript.

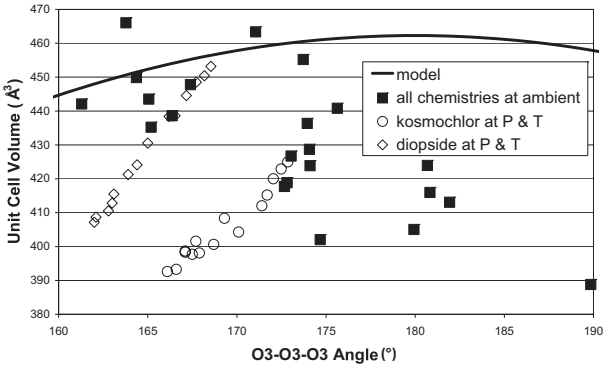

FIGURE 3. A plot of the relationship between unit-cell volume and O3-O3-O3 angle for 22 ambient condition $C2/c$ pyroxenes taken from the literature (solid data points, references in Table 1) and for a model pyroxene with model oxygen radius of 4/3 Å (solid line). Data for diopside at P (Downs and Thompson, in prep) and T (Cameron et al. 1973) and kosmochlor at P (Origlieri et al. 2003) and T (Cameron et al. 1973) are denoted by open symbols.

the mixing volume is proportional to the number of M1 octahedral edges shared between octahedra with different chemistries, related to the strain resulting from the mismatch in cation sizes. Using probability theory (cf. Olkin et al. 1980), if there are only two M1 cations, then the relative frequency of such shared edges is $2X(1 - X)$, where X is the mole fraction of one of the cations. Therefore, if the mixing volume is proportional to the number of M1 octahedral edges shared between octahedra with different chemistries, then mixing volume should be proportional to $2X(1 - X)$, i.e., $V_{mix} = 2kX(1 - X)$, where k is a proportionality constant.

Figure 4 is a plot of the relationship between mixing volume and relative frequency of shared edges between M1 octahedra with different chemistries for various compositions along the diopside-hedenbergite join ($CaMgSi_2O_6$-$CaFeSi_2O_6$). The four intermediate composition data points are from Raudsepp et al. (1990a). The diopside volume is the average of the room condition volumes from Levien and Prewitt (1981) and Cameron et al. (1973); the hedenbergite volume is the average of the room condition volumes from Zhang et al. (1997) and Cameron et al. (1973). The resulting equation is $V_{mix} = 4X(1 - X)$, where X is the mole fraction of one of the cations, i.e., proportionality constant $k = 2$.

Table 2 contains data and references for 18 pyroxene binary solid solutions taken from the literature. The M1 chemistry varies in 16 of these solutions, in some instances coupled with other substitutions. In nine of these 16 series, the data show no systematic relationship between mixing volume and composition. Five series have relationships between mixing volume and composition that are consistent with the above hypothesis (R^2 = 0.99, 0.98, 0.97, 0.96, 0.95), but two of these have only two intermediate composition data points. Only one series displays a clear systematic relationship between mixing volume and composition where that relationship is inconsistent with the above hypothesis. The one remaining series has a mixing volume-composition relationship that is difficult to interpret as definitively systematic or not systematic.

Two of the 18 binary solid solutions in Table 2 have fixed M1 chemistry. The first is a portion of the diopside-enstatite series [$CaMgSi_2O_6$-$(Ca_{0.5}Mg_{0.5})MgSi_2O_6$], while the second is the entire series. All members of the first series have space group $C2/c$, while the two additional members of the second series have space group $P2_1/c$. Mixing volumes for the $C2/c$ portion of the diopside-enstatite series are very small, 0.13% of unit-cell volume or less. Mixing volumes over the entire series are much larger, with some members having mixing volumes over 1% of the unit-cell volume.

The sizes of the mixing volumes in all of the examined $C2/c$ pyroxene series are very small. The largest mixing volume in absolute value from the 17 $C2/c$ series examined is 1.61 Å^3, or 0.36%, in the $NaVSi_2O_6$-$CaMnSi_2O_6$ series.

Volume variation with *P* and *T*

The TD model is usefully applied to the analysis of unit-cell volume variation with pressure and temperature. In Figure 3, data determined at P and T are indicated by open symbols and demonstrate that changes in unit-cell volume with P and T in diopside (P = Downs and Thompson, in prep; T = Cameron et al. 1973) and kosmochlor (P = Origlieri et al. 2003; T = Cameron et al. 1973) are positively correlated with the O3-O3-O3 angle, θ, in a well-defined trend. This positive correlation is similar to that of the model, but with steeper slopes. The model volume change is due only to tetrahedral rotation, since the model oxygen radius, r, is kept fixed in this plot. The steeper slope of the observed data is consistent with additional variation due to changes in the oxygen radius. Because the model is parameterized in terms of θ and r, we can calculate the contributions of changes in these two parameters toward volume change.

In the following example, the model is applied to diopside at pressure (Downs and Thompson, in prep). The first step is to produce a model pyroxene with the same θ and unit-cell volume as ambient diopside (Table 3). This is calculated by setting the model θ to the observed value, and varying the model r until the observed unit-cell volume is reproduced. Next, another model pyroxene with the same model oxygen radius, but θ from 10.16

TABLE 2. Mixing volume data for some binary solid-solution series taken from the literature

Chemistry	CWH	$\%V_{mix}$	Reference
$CaMgSi_2O_6$-$CaFeSi_2O_6$	Y	0.23	Cameron et al. (1973) Levien and Prewitt (1981) Raudsepp et al. (1990a) Zhang et al. (1997)
$CaMgSi_2O_6$-$CaAl(AlSi)O_6$	Y	0.37	Cameron et al. (1973) Okamura et al. (1974) Levien and Prewitt (1981) Tribaudino (1996)
$CaMgSi_2O_6$-$CaNiSi_2O_6$	I	0.13	Raudsepp et al. (1990b)
$CaFe^{2+}Si_2O_6$-$NaFe^{3+}Si_2O_6$	I	0.23	Redhammer et al. (2000)
$CaMgSi_2O_6$-$NaAlSi_2O_6$	I	0.16	Wood et al. (1980)
$CaMgSi_2O_6$-$CaZnSi_2O_6$	N	0.26	Ohashi et al. (2003a)
$NaInSi_2O_6$-$NaScSi_2O_6$	Y	0.04	Ohashi et al. (1990, 1994a, 2003b)
$NaTiSi_2O_6$-$CaMgSi_2O_6$	I	0.25	Levien and Prewitt (1981) Ohashi et al. (1982, 2003c)
$NaVSi_2O_6$-$CaMnSi_2O_6$	Y	0.36	Ohashi et al. (1994b, 2003d)
$NaVSi_2O_6$-$CaMgSi_2O_6$	Y	0.25	Levien and Prewitt (1981) Ohashi et al. (1994b, 2003e)
$NaCrSi_2O_6$-$CaMgSi_2O_6$	I	0.13	Levien and Prewitt (1981) Ohashi et al. (2003f,g)
$NaGaSi_2O_6$-$NaAlSi_2O_6$	I	0.08	Ohashi et al. (2003h)
$NaGaSi_2O_6$-$NaScSi_2O_6$	I	0.25	Ohashi et al. (1995,2003i)
$LiGaSi_2O_6$-$LiAlSi_2O_6$*	I?	0.14	Sato et al. (1994) Arlt and Angel (2000) Ohashi et al. (2003j)
$LiFeSi_2O_6$-$LiScSi_2O_6$	I	0.13	Redhammer and Roth (2004)
$LiScSi_2O_6$-$LiInSi_2O_6$	I	0.11	Redhammer and Roth (2004)
$CaMgSi_2O_6$-$(Ca_{0.5}Mg_{0.5})MgSi_2O_6$	N/A	0.13	Tribaudino et al. (2000) Tribaudino (2000)
$CaMgSi_2O_6$-$MgMgSi_2O_6$†	N/A	1.18	Ohashi (1984) Tribaudino et al. (2000, 2002) Tribaudino (2000)

Notes: If the mixing volumes for a series are proportional to the relative frequency of shared edges between M1 octahedra with different chemistries across that series, then there is a Y for Yes in the column labeled CWH (Consistency With Hypothesis); if there is a systematic relationship between mixing volume and chemistry, but mixing volume is not proportional to the relative frequency of shared edges between M1 octahedra with different chemistries across that series, then there is an N for No in the column labeled CWH; if there is no systematic relationship between mixing volume and chemistry, then there is an Inconclusive in the column labeled CWH; if M1 chemistry is fixed across the series, then there is a Not/Applicable in the column labeled CWH. Data in the column labeled $\%V_{mix}$ ($= |V_{mix}|/V \times 100$) are the maximum percentage mixing volumes for each series. Mixing volumes for $C2/c$ pyroxenes are very small, all less than 0.4% of the unit-cell volume.

* This end-member has space group $P2_1/c$, all intermediates are $C2/c$.

† This end-member and the $Ca_{0.15}$ intermediate member have space group $P2_1/c$.

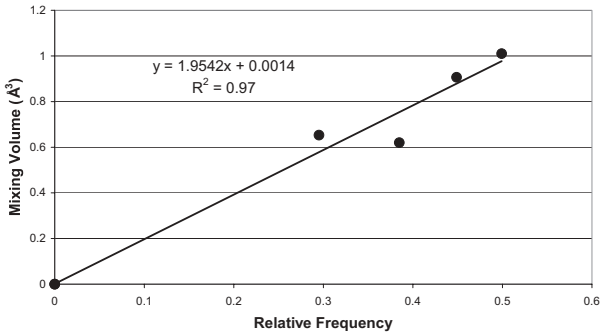

FIGURE 4. A plot of the relationship between mixing volume and relative frequency of edges shared by M1 octahedra with different chemistries for the diopside-hedenbergite join. The four intermediate composition data points are from Raudsepp et al. (1990b). The diopside volume is the average of the room condition volumes from Levien and Prewitt (1981) and Cameron et al. (1973); hedenbergite volume is the average of the room condition volumes from Zhang et al. (1997) and Cameron et al. (1973). The resulting equation is $V_{mix} = 4X(1 - X)$, where X is the mole fraction of one of the cations.

GPa, is calculated. The change in volume between the two model pyroxenes is therefore due entirely to tetrahedral rotation. Comparing the change in the model with the observed change suggests that tetrahedral rotation alone accounts for approximately 19% of the observed volume decrease.

Analysis of changes in the M1 octahedral volume can be used to quantitatively estimate the contribution of changes in r (i.e., isotropic compression) to the total observed volume decrease. The near regularity of the observed M1 octahedra (Table 4) suggests that they will exhibit model behavior, i.e., their volume decrease will be due only to a combination of tetrahedral rotation and isotropic compression. Assuming that the observed M1 volume decrease due to isotropic compression is a valid measure of the isotropic compression of the crystal as a whole, and that the magnitude of the observed M1 volume decrease due to tetrahedral rotation is approximately that of the model, then approximately 77% of the observed volume decrease is due to isotropic compression.

This suggests that most of the anisotropy of compression, i.e., the size and shape of the strain ellipsoid, is due to tetrahedral rotation. Consistent with this, Thompson and Downs (2004) found that the TD model largely reproduces the strain ellipsoids for observed pyroxenes.

The remaining 4% of the observed volume decrease is probably due to changes in the distortion of the observed pyroxene from the model. For instance, the b/c ratio in all model pyroxenes is constant at $\sqrt{3} = 1.7321$, but is observed to change from 1.699 to 1.687 in diopside between 0 and 10.16 GPa.

Figure 5 illustrates that the TD model can reproduce the volume vs. θ relationship for diopside at P (Downs and Thompson, in prep) and T (Cameron et al. 1973) using simple representations of r and θ as linear in P and T. The TD model relations at P (GPa) and T (°C) were calculated as follows. First, equations for θ as functions of P and T were derived from experimental data:

$$\angle\text{O3-O3-O3} = -0.4192P + 166.22,\ R^2 = 0.99$$
$$\angle\text{O3-O3-O3} = 0.0022T + 166.3,\ R^2 = 0.99$$

TABLE 3. Structural data for diopside at 0 and 10.16 GPa from Downs and Thompson (in prep) and two model pyroxenes

		D & T	D & T	Model 1	Model 2
condition		0 GPa	10.16 GPa		
V (Å^3)		438.63(3)	407.16(3)	438.63	432.60
∠O3-O3-O3		166.53(9)	162.0(2)	166.53	162.0
M1 V (Å^3)		11.82	10.89	13.02	12.81
a		9.7397(3)	9.5164(5)	9.7568	9.6877
b		8.9174(3)	8.6449(4)	9.0676	9.0182
c		5.2503(2)	5.1246(3)	5.2352	5.2067
β		105.866(3)	103.76(5)	108.73	108.01
T	x	0.286187(55)	0.28610(17)	0.30823	0.30840
	y	0.093189(55)	0.09554(14)	1/12	1/12
z		0.229355(99)	0.22718(23)	0.26780	0.26073
M1	y	0.908083(97)	0.91075(24)	11/12	11/12
M2	y	0.301478(61)	0.30587(16)	1/4	1/4
O1	x	0.11554(15)	0.11538(43)	0.13354	0.13320
	y	0.08690(15)	0.08832(35)	1/12	1/12
	z	0.14186(27)	0.14178(59)	0.16326	0.15996
O2	x	0.36094(15)	0.35921(45)	0.36646	0.36680
	y	0.25019(15)	0.25714(40)	1/4	1/4
	z	0.31766(27)	0.32226(59)	0.33674	0.34004
O3	x	0.35073(14)	0.35409(46)	0.36646	0.36680
	y	0.01744(15)	0.02340(36)	0.01705	0.02286
	z	0.99543(26)	0.98725(61)	0.03561	0.02146

Notes: The first model is the model equivalent to the 0 GPa diopside. It has the same unit-cell volume and tetrahedral chain geometry (i.e., O3-O3-O3 angle). The second model has the tetrahedral chain geometry of the 10.16 GPa diopside, but it has the same model oxygen radius as the first model. This means that the volume decrease in the second model is due strictly to rotation of the tetrahedra.

TABLE 4. Some data for diopside (Downs and Thompson, in prep) showing that the M1 octahedron is very regular

P (GPa)	M1 angle variance	M1 quadratic elongation
0	17.790	1.0054
10.16	16.990	1.0051

Note: Measures of polyhedral distortion are from Robinson et al. (1971).

We assume that these relationships are valid from 0 to 10.16 GPa, and 24 to 1000 °C. Second, equations for the model oxygen radius of diopside, r, as functions of P and T were derived from the calculated model equivalents of the lowest and highest pressure (Table 3) and temperature structures:

$$r = -0.0025944\ P + 1.3179\ \text{Å}$$
$$r = 0.000012443\ T + 1.3180\ \text{Å}$$

Values were calculated at 1 GPa and 100 °C increments over the domains of interest. The unit-cell volumes for the models with these angles and model radii were calculated using the formula from Thompson and Downs (2004),

$$V = [32\sqrt{2}(1 - \cos\theta) + 64(1 - \cos\theta)^{3/2}/\sqrt{3}]r^3 \quad (1)$$

The ability to predict volume at pressure or temperature from ambient condition volume alone is desirable because P and T experiments are difficult and time-consuming. Here we combine the simple modeling of θ and r as linear in P with the volume-composition relationship derived previously to predict V as a function of P for the calcium pyroxenes from a single set of equations:

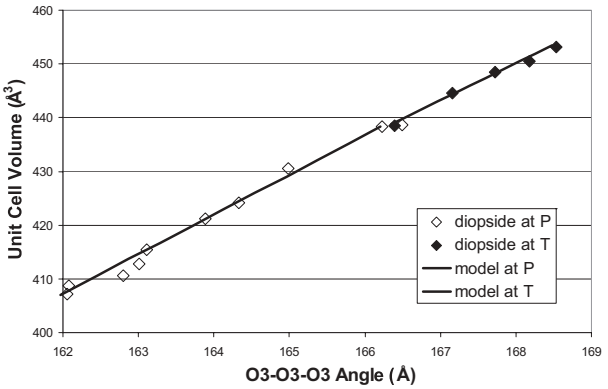

FIGURE 5. A plot of the relationship between unit-cell volume and O3-O3-O3 angle for diopside at *P* (Downs and Thompson, in prep.) and *T* (Cameron et al. 1973) and model diopsides with linearly varying O3-O3-O3 angles and model oxygen radii as functions of *P* and *T*. This demonstrates that the combination of tetrahedral rotation and isotropic compression or expansion can model the behavior of pyroxenes with *P* and *T*.

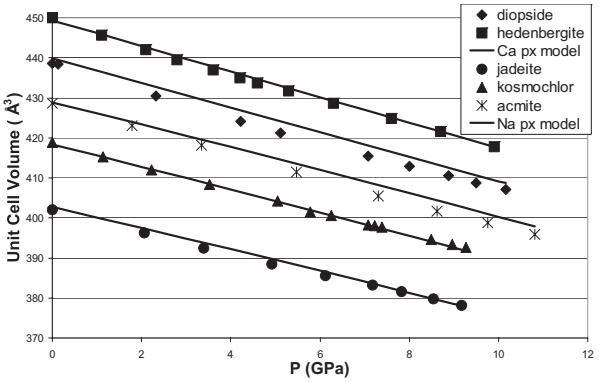

FIGURE 6. A comparison of the *V* vs. *P* curves for the experimental data and a simple model that can be calculated from ambient structural data using one equation with one set of coefficients for the sodium pyroxenes, and another for the calcium pyroxenes. The model is a reasonable first approximation, but does not reproduce bulk moduli or the observed curvature in *PV* data well. Observed data for diopside and jadeite are from Downs and Thompson (in prep.), acmite is from Downs et al. (in prep.), hedenbergite is from Zhang et al. (1997), and kosmochlor is from Origlieri et al. (2003).

$r_o = m_1 V_o + b$, where V_o = ambient unit-cell volume,
$r = m_2 P + r_o = m_2 P + m_1 V_o + b$,
$\theta = m_3 P + \theta_o$.

The coefficient set is $[m_1, b, m_2, m_3]_{Ca}$ = [0.00107325, 0.848365, –0.00255913, –0.442600], and was derived from experimental data. The values of *r* and θ calculated this way are plugged into Equation 1. Figure 6 compares the model with actual data for diopside (Downs and Thompson, in prep), hedenbergite (Zhang et al. 1997), jadeite (Downs and Thompson, in prep), acmite (Downs et al., in prep), and kosmochlor (Origlieri et al. 2003). The curves for the sodium pyroxenes were computed as above using the coefficient set $[m_1, b, m_2, m_3]_{Na}$ = [0.00102327, 0.863203, –0.00241210, –0.703133]. While this approach produces reasonable first approximations, it does not reproduce important properties such as the bulk modulus and its derivatives because *r* and θ are not truly linear in *P*.

The model can accurately reproduce bulk moduli and their derivatives when *r* and θ are represented as quadratic in *P*, and fit to a specific data set (i.e., separate equations are needed to model each pyroxene). Quadratic representations were chosen for ease of use and quality of fit, not because of physical or theoretical considerations. This limits the ability of this version of the model to extrapolate to very high pressures. For instance, the diopside *r* and θ quadratics have minima at approximately 35 and 24 GPa, respectively. Therefore, model volumes begin increasing above 32 GPa. Figure 7 illustrates this by comparing the model volumes for diopside derived from the data of Downs and Thompson (in prep) to the unit-cell volume data of Tribaudino et al. (2000) up to 41 GPa. Different functional forms for *r*(*P*) and θ(*P*) derived from theory, or arbitrary representations such as quadratics, fit to higher pressure structural determinations, are needed to make the model reliable at very high pressures.

Coefficients for the quadratics are given in Table 5. The quadratics for *r* were derived by making model equivalents to each pressure structure, and fitting a quadratic to the *r*'s obtained from

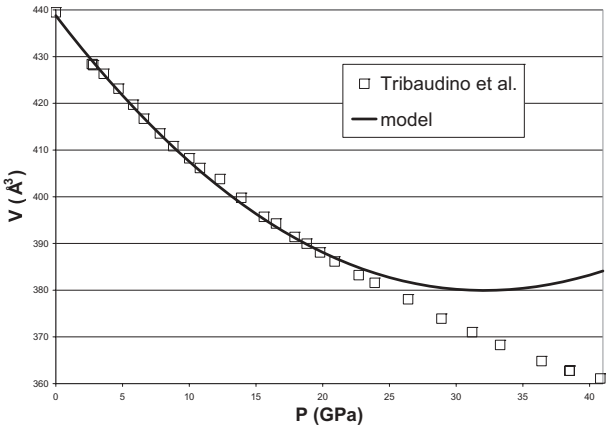

FIGURE 7. Model limitations due to the arbitrary representation of the model oxygen radius and O3-O3-O3 angle as quadratic in *P* are illustrated by comparing the model volumes for diopside derived from the data of Downs and Thompson (in prep.) to the unit-cell volume data of Tribaudino et al. (2000) up to 41 GPa. Different functional forms for *r*(*P*) and θ(*P*) derived from theory, or arbitrary representations such as quadratics, fit to higher pressure structural determinations, are needed to make the model reliable at very high pressures.

these models. However, there is a lot of scatter in the observed θ data, so the coefficients for the θ quadratics were optimized to give the least-squares best fit between model and observed volumes, using a minimizer described by Dennis and Schnabel (1983) and coded by L. Johnson and M. Boisen. Figure 8 shows that the resulting equations for θ (solid black lines) fit the data well, i.e., are physically realistic. Figure 9 illustrates the fit between the model *V* vs. *P* curves and the data.

Table 6 compares third-order Birch-Murnaghan fits to the observed data and the calculated model volumes. The Birch-Murnaghan K_o and K' values for the computed and observed volumes are statistically identical.

The analytic expression for $V(P)$, given in Equation 1 can be used to calculate values for the room pressure bulk modulus, K_o, and to derive expressions for the bulk modulus, K, and its pressure derivatives as functions of pressure. The equations to calculate K, K', and K'' as functions of pressure are as follows:

$$\theta = a_\theta P^2 + b_\theta P + c_\theta, \text{ coefficients specific to each pyroxene are in Table 5}$$

$$r = a_r P^2 + b_r P + c_r$$

$$V = [32\sqrt{2}(1 - \cos\theta) + 64(1 - \cos\theta)^{3/2}/\sqrt{3}]r^3$$

$$V' = 3Vr'/r + r^3[32\sqrt{2}\sin(\theta)\theta' + 32\sqrt{3}(1 - \cos\theta)^{1/2}\sin(\theta)\theta']$$

$$V'' = (3Vr'' + 6V'r')/r - 12Vr'^2/r^2 + r^3(32\sqrt{2}[\cos(\theta)\theta'^2 + \sin(\theta)\theta''] + 32\sqrt{3}[1 - \cos\theta]^{1/2}A),$$

where $A = \sin^2(\theta)\theta'^2/[2(1 - \cos\theta)] + \cos(\theta)\theta'^2 + \sin(\theta)\theta''$

$$V''' = 9(V''r' + V'r'')/r - 36r'(Vr'' + V'r')/r^2 + 60Vr'^3/r^3 + r^3(32\sqrt{2}[-\sin(\theta)\theta'^3 + 3\cos(\theta)\theta'\theta''] + 32\sqrt{3}(\sin(\theta)\theta'A/[2(1 - \cos\theta)^{1/2}] + [1 - \cos\theta]^{1/2}A')),$$

where $A' = -\sin^3(\theta)\theta'^3/[2(1 - \cos\theta)^2] + \sin(2\theta)\theta'^3/[2(1 - \cos\theta)] + \sin^2(\theta)\theta'\theta''/(1 - \cos\theta) - \sin(\theta)\theta'^3 + 3\cos(\theta)\theta'\theta''$

$$K = -V/V'$$

$$K' = -1 - KV''/V'$$

$$K'' = -(K'V'' + KV''' - KV''^2/V')/V'$$

Table 7 gives results for five pyroxenes at 0, 5, 10, and 15 GPa.

A comparison of Tables 6 and 7 shows that the TD room pressure bulk moduli (calculated from the analytic expressions) are larger than the Birch-Murnaghan room pressure bulk moduli (obtained by fitting to experimental data) by about 3 GPa and that the TD bulk modulus first pressure derivatives start smaller than the Birch-Murnaghan pressure first derivatives (assumed to be

TABLE 5. Coefficients of the quadratics used to model the model oxygen radii, *r*, and O3-O3-O3 angles, θ

	r			
P	$a_r \times 10^5$ (Å/GPa²)	$b_r \times 10^3$ (Å/GPa)	c_r (Å)	R^2
diopside	4.40(82)	−3.096(84)	1.31824(17)	1.000
hedenbergite	2.24(1.40)	−2.736(145)	1.33150(32)	0.998
jadeite	4.15(2.60)	−2.728(256)	1.27382(54)	0.995
acmite	4.59(1.74)	−3.014(197)	1.30212(45)	0.997
kosmochlor	1.93(1.66)	−2.521(164)	1.29200(35)	0.997
T	$a_r \times 10^9$ (Å/°C²)	$b_r \times 10^6$ (Å/°C)	c_r (Å)	
diopside	−0.98(1.75)	13.10(1.83)	1.31776(40)	0.997
hedenbergite	4.16(1.18)	4.72(1.25)	1.33229(29)	0.996
jadeite	1.69(1.27)	8.63(1.06)	1.27348(19)	0.999
acmite	3.68(4.19)	7.36(3.49)	1.30188(61)	0.991
kosmochlor	4.22	5.36	1.29389	1
		θ		
P	a_θ (°/GPa²)	b_θ (°/GPa)	c_θ (°)	rmse
diopside	0.01081	−0.5249	166.334	0.156
hedenbergite	0.01813	−0.6480	164.420	0.168
jadeite	0.00627	−0.7021	174.673	0.533
acmite	0.00463	−0.8283	173.760	0.414
kosmochlor	0.02199	−0.9354	173.153	0.534
T	$a_\theta \times 10^7$ (°/°C²)	$b_\theta \times 10^4$ (°/°C)	c_θ (°)	
diopside	3.80	17.93	166.353	0.036
hedenbergite	−12.60	42.20	164.370	0.039
jadeite	8.26	3.0842	174.582	0.030
acmite	9.75	0.3514	173.997	0.021
kosmochlor	11.84	6.6363	172.027	0.000

Note: The O3-O3-O3 angle quadratic coefficients were optimized to create the best fit between model and observed volumes because of scatter in the data, so rmse values are reported in lieu of coefficient standard deviations. The model oxygen radius for kosmochlor at temperature has no errors reported because there are only three data points, so the quadratic fit is perfect. All values for high-*T* coefficients derived from the experimental data of Cameron et al. (1973); high-*P* diopside and jadeite from Downs and Thompson (in prep.); high-*P* acmite from Downs et al. (in prep.); high-*P* hedenbergite from Zhang et al. (1997); high-*P* kosmochlor from Origlieri et al. (2003).

TABLE 6. A comparison of the third order Birch-Murnaghan fits to the observed volumes and the calculated model volumes

	K_o (GPa)	K_o' (GPa/P)
Observed diopside	115.6(1.5)	4.2(3)
Model diopside	115.6(6)	4.2(1)
Observed hedenbergite	120.2(2.3)	3.3(5)
Model hedenbergite	120.1(5)	3.4(1)
Observed jadeite	136.5(1.4)	3.4(4)
Model jadeite	138.0(4)	3.0(1)
Observed acmite	125.1(4.5)	1.9(7)
Model acmite	123.9(4)	2.1(1)
Observed kosmochlor	136.5(3.2)	1.7(6)
Model kosmochlor	136.7(6)	1.7(1)

Notes: The model reproduces the room pressure bulk modulus and its first derivative, K_o and K_o', within error. References for the experimental data are: high-*P* diopside and jadeite from Downs and Thompson (in prep); high-*P* acmite from Downs et al. (in prep); high-*P* hedenbergite from Zhang et al. (1997); high-*P* kosmochlor from Origlieri et al. (2003).

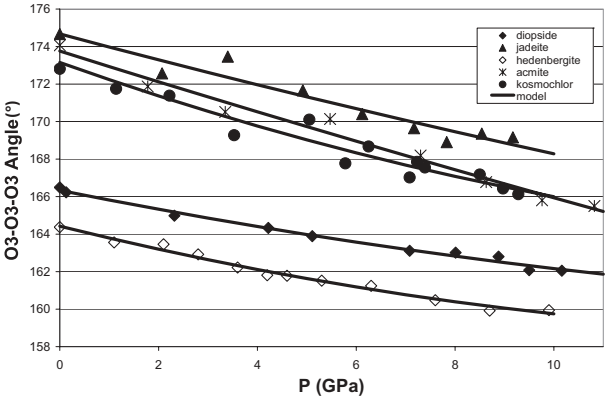

FIGURE 8. A plot of the fit of model O3-O3-O3 angle quadratics and the experimental data showing that the optimized quadratics are physically realistic. Observed data for diopside and jadeite are from Downs and Thompson (in prep.), acmite is from Downs et al. (in prep), hedenbergite is from Zhang et al. (1997), and kosmochlor is from Origlieri et al. (2003).

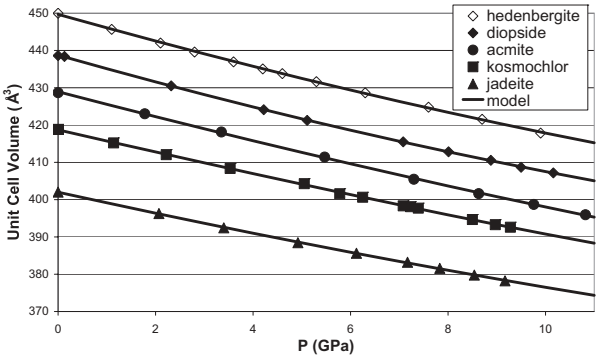

FIGURE 9. A V vs. P plot of the fit of the model to the observed data when the O3-O3-O3 angles and model oxygen radii are represented as quadratics in P. Observed data for diopside and jadeite are from Downs and Thompson (in prep.), acmite is from Downs et al. (in prep.), hedenbergite is from Zhang et al. (1997), and kosmochlor is from Origlieri et al. (2003).

constant) and increase rapidly with pressure. Table 8 compares the mean square error for both models showing that they fit the observed data equally well.

A more detailed analysis of jadeite (Downs and Thompson, in prep) illustrates subtle differences between the two models in their description of pyroxene behavior, although volume vs. pressure curves for the two models appear nearly identical (Fig. 10). The analytical expression for the third-order Birch-Murnaghan equation can be used to calculate the bulk modulus, K, and its first derivative as a function of volume using as parameters the values for room pressure bulk modulus and its derivative, K_o and K_o', as follows:

$$A = (V_o/V)^{7/3} - (V_o/V)^{5/3}$$
$$A'/V' = (-7/3)V_o^{7/3}V^{-10/3} + (5/3)V_o^{5/3}V^{-8/3}$$
$$B = 1 - (3/4)(4 - K_o')[(V_o/V)^{2/3} - 1]$$
$$B'/V' = (1/2)(4 - K_o')\ V_o^{2/3}V^{-5/3}$$
$$P = 1.5K_oAB$$
$$K = -1.5K_oV(BA'/V' + A\,B'/V')$$
$$K' = (1.5K_oV^2/K)[2(B'/V')(A'/V') + B[(70/9)V_o^{7/3}V^{-13/3} + (40/9)V_o^{5/3}V^{-11/3}] + A(-5/6)(4 - K_o')\ V_o^{2/3}V^{-8/3}] - 1$$

The parameters used in the Birch-Murnaghan analytic expression for jadeite (Downs and Thompson, in prep) were obtained by a least-squares fit to the observed data and are as follows: V_o = 402.030 Å^3, K_o = 136.5 GPa, K_o' = 3.37. Table 9 contains the observed PV data, and the model volumes, bulk moduli, and first derivatives for both models. A difference between the models is that the Birch-Murnaghan bulk modulus first pressure-derivative actually decreases slightly with pressure (i.e., $K'' < 0$, the rate at which the structure gets stiffer decreases), while the TD first pressure-derivative increases with pressure (i.e., $K'' > 0$, the structure gets stiffer more rapidly as pressure increases), which may be less physically realistic.

The relationship between ambient unit-cell volume and M1 cation radius suggests that bulk compressibility in $C2/c$ silicate pyroxenes may be controlled by the compressibility of the M1 octahedron. This is consistent with the findings of Tribaudino et al. (2001) that M2 chemistry has little effect on the bulk modulus along the diopside-enstatite join.

Volume at simultaneous P and T

The TD model can be used to estimate the unit-cell volumes of these pyroxenes at simultaneous P and T. This is done by straightforward substitution of θ and r temperature quadratics for the constant term in the pressure quadratics (i.e., heat up the model pyroxene, then squeeze it). This formulation works well despite the absence of cross terms in P and T.

Quadratics for θ and r as functions of T (Table 5) were derived from the data of Cameron et al. (1973). These are substituted into the pressure quadratics for the c coefficient (θ_o and r_o), resulting in the following equations:

$$\theta(P,T) = a_{\theta P}P^2 + b_{\theta P}P + a_{\theta T}T^2 + a_{\theta T}T + c_{\theta T}$$
$$r(P,T) = a_{rP}P^2 + b_{rP}P + a_{rT}T^2 + a_{rT}T + c_{rT}.$$

Values calculated from these equations are then substituted into Equation 1. The P and T coefficients for each pyroxene are given in Table 5.

For example, the coefficients for diopside were obtained from Table 5 giving the following equations:

TABLE 7. Results of calculations using the analytic expression for $V(P)$ to get information on the bulk modulus, K, and its derivatives as functions of pressure.

	P (GPa)	K (GPa)	K'	K'' (GPa^{-1})
diopside	0	118.5	2.6	0.23
	5	135.0	4.1	0.36
	10	160.9	6.5	0.66
	15	204.0	11.3	1.40
hedenbergite	0	123.1	1.8	0.27
	5	135.5	3.3	0.35
	10	156.8	5.4	0.54
	15	192.1	9.0	0.95
jadeite	0	139.9	1.9	0.18
	5	152.1	3.0	0.25
	10	170.6	4.5	0.39
	15	199.0	7.1	0.68
acmite	0	125.9	1.2	0.11
	5	133.3	1.8	0.14
	10	144.3	2.6	0.20
	15	160.4	3.9	0.30
kosmochlor	0	141.0	–0.7	0.49
	5	143.3	1.5	0.42
	10	156.4	3.8	0.50
	15	182.4	6.8	0.76

Note: Model parameters were fit to the experimental data of: high-P diopside and jadeite from Downs and Thompson (in prep.); high-P acmite from Downs et al. (in prep.); high-P hedenbergite from Zhang et al. (1997); high-P kosmochlor from Origlieri et al. (2003).

TABLE 8. A comparison of the mean square error (Å^6) for the fits of the unit-cell volumes calculated with the Thompson and Downs (TD) model and the Birch-Murnaghan (BM) model to the observed data, showing that they both fit the data equally well

	TD	BM
diopside	0.007	0.008
hedenbergite	0.031	0.021
jadeite	0.015	0.014
acmite	0.041	0.048
kosmochlor	0.026	0.024

Notes: Models were fit to the experimental data of: high-P diopside and jadeite from Downs and Thompson (in prep.); high-P acmite from Downs et al. (in prep.); high-P hedenbergite from Zhang et al. (1997); high-P kosmochlor from Origlieri et al. (2003).

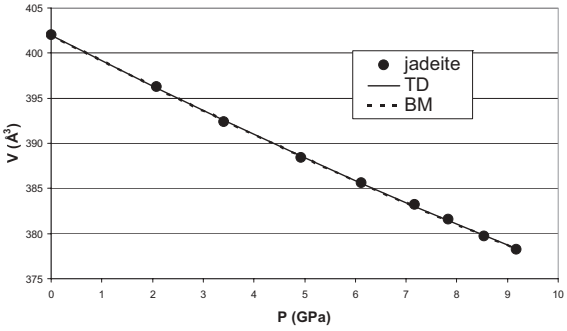

FIGURE 10. A plot of the fits of the Thompson and Downs (TD) model and the third-order Birch-Murnaghan (BM) model to the observed jadeite data (Downs and Thompson, in prep).

$$\theta(P,T) = 0.01081480P^2 - 0.5249419P + 3.804013E{-}7T^2 + 17.92897E{-}4T + 166.35334$$
$$r(P,T) = 4.39994E{-}5P^2 - 3.09581E{-}3P - 0.976586E{-}9T^2 + 13.1004E{-}6T + 1.3177634.$$

$\theta(P,T)$ and $r(P,T)$ can now be calculated for arbitrary P and T and substituted into:

$$V[\theta(P,T), r(P,T)] = (32\sqrt{2}[1 - \cos\theta(P,T)] + 64[1 - \cos\theta(P,T)]^{3/2}/\sqrt{3})r(P,T)^3.$$

Zhao et al. obtained unit-cell volumes for jadeite (1997) and diopside (1998) at 31 different points in *PT*-space. The model derived from the room *T*, high-*P* data of Downs and Thompson (in prep) and the room *P*, high-*T* data of Cameron et al. (1973) matched the observed unit-cell volumes with an average error of 0.19% for jadeite (Table 10, Fig. 11) and 0.48% for diopside (Fig. 10). Figure 12 shows that there is a systematic error in the model because it was not fit to structural data from the Zhao et al. (1997, 1998) experiment, which was not reported. There is additional uncertainty because there is no zero-pressure isobar in Zhao's data to compare with the Cameron et al. (1973) data that the model was also fit to. However the effect appears small, especially for jadeite. The structural data used to derive the model was from single-crystal, diamond-anvil cell, four-circle X-ray diffractometer experiments, while Zhao et al.'s (1997, 1998) powder cell parameter data was from multi-anvil, synchrotron powder diffraction that only produced cell parameters. With structural information from the Zhao et al. (1997, 1998) experiment, information about the coefficients in the pressure quadratics as functions of temperature might have been determined. They are probably not constants with temperature as calculations show that the model β decreases slightly with temperature, while Zhao et al.'s (1997, 1998) data suggest it should increase, i.e., Zhao's isotherms trend toward convergence, while the TD model isotherms are close to parallel.

Figure 13 shows *V* vs. *P* isotherms for hedenbergite, acmite, jadeite, and kosmochlor calculated from the model. Isotherms are for ambient temperature, 200, 400, 600, 800, and 1000 °C.

TABLE 9. Observed *PV* data for jadeite (Downs and Thompson, in prep) with model volumes, bulk moduli (*K*), and first derivatives (*K'*) calculated from both the Thompson and Downs (TD) model and the third order Birch-Murnaghan (BM) model

P (GPa)	*V* (Å³)	V_{TD}	K_{TD}	K'_{TD}	V_{BM}	K_{BM}	K'_{BM}
0.0001	402.03(2)	401.993	139.91	1.94	402.030	136.52	3.37
2.07	396.28(4)	396.177	144.32	2.33	396.129	143.27	3.32
3.40	392.43(4)	392.583	147.60	2.61	392.527	147.96	3.29
4.92	388.44(5)	388.616	151.83	2.96	388.578	152.99	3.25
6.12	385.61(4)	385.593	155.56	3.27	385.577	156.66	3.23
7.17	383.23(3)	383.028	159.15	3.57	383.029	159.82	3.21
7.83	381.57(5)	381.454	161.57	3.77	381.464	162.05	3.20
8.54	379.77(3)	379.796	164.33	4.00	379.809	164.52	3.18
9.17	378.23(3)	378.354	166.92	4.22	378.366	166.65	3.17

Notes: The parameters used in the BM analytic expression were obtained by a least-squares fit to the observed data and follow: V_o = 402.030(020) Å³, K_o = 136.5(1.4) GPa, K_o' = 3.37(41).

Volumes at *P*, *T*, and *x*

As discussed previously, mixing volumes are small, and so these equations can be combined in an uncoupled way to produce reasonable volume data at *P* and *T* for *C*2/*c* pyroxenes with mixed M cation occupancies, thus establishing a means to predict density at depth in the mantle for many pyroxenes of arbitrary chemistry. For example, suppose a model volume is needed for a pyroxene at 1373 °C and 10.1 GPa, whose composition is a solid solution with components 81.2% diopside, 13.0% hedenbergite, and 5.8% jadeite. We start with the equations

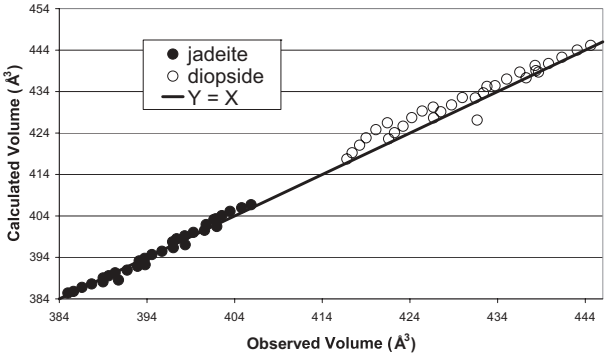

FIGURE 11. A comparison of model unit-cell volumes for jadeite and diopside, calculated at 31 points in *PT* space for each pyroxene, with the experimental data of Zhao et al. (1997, 1998). The average error was 0.19% and 0.48%, respectively.

TABLE 10. Comparison of Zhao et al.'s (1997) *PTV* data for jadeite with the model derived from Downs and Thompson's (in prep.) room *T*, high-*P* data, and Cameron et al.'s (1973) room *P*, high-*T* data

T (°C)	*P* (GPa)	V_{obs} (Å³)	V_{calc} (Å³)	$\lvert V_{obs} - V_{calc} \rvert$	%
27	0	403.32(8)	401.86	1.46	0.36%
1007	8.16	388.54(9)	390.74	2.20	0.57%
799	7.83	388.12(9)	388.99	0.87	0.22%
601	7.44	387.59(9)	387.69	0.10	0.02%
397	7.02	386.79(9)	386.59	0.20	0.05%
200	6.65	385.80(9)	385.62	0.18	0.05%
35	6.33	385.41(9)	384.98	0.43	0.11%
1007	6.88	392.23(9)	393.79	1.56	0.40%
799	6.2	391.85(9)	392.93	1.08	0.28%
599	5.78	390.93(9)	391.73	0.80	0.21%
399	5.5	390.28(9)	390.37	0.09	0.02%
198	5.04	389.57(9)	389.63	0.06	0.02%
34	4.73	389.06(9)	389.01	0.05	0.01%
1005	5.03	397.06(9)	398.36	1.30	0.33%
799	4.59	396.36(6)	397.01	0.65	0.16%
599	4.23	395.49(9)	395.70	0.21	0.05%
400	3.88	394.69(9)	394.56	0.13	0.03%
199	3.47	393.77(9)	393.74	0.03	0.01%
34	3.17	393.16(9)	393.11	0.05	0.01%
1003	3.63	401.46(8)	401.97	0.51	0.13%
800	3.24	400.53(9)	400.56	0.03	0.01%
600	2.88	400.05(9)	399.30	0.75	0.19%
399	2.48	399.20(9)	398.31	0.89	0.22%
198	2.12	398.51(9)	397.38	1.13	0.28%
35	1.77	397.76(5)	396.93	0.83	0.21%
1002	2.17	406.70(6)	405.87	0.83	0.20%
800	1.68	405.97(7)	404.81	1.16	0.29%
600	1.36	405.12(9)	403.47	1.65	0.41%
398	0.95	404.08(6)	402.54	1.54	0.38%
200	0.61	403.15(7)	401.62	1.53	0.38%
35	0.41	401.94(9)	400.75	1.19	0.30%

Note: Average error is 0.19%.

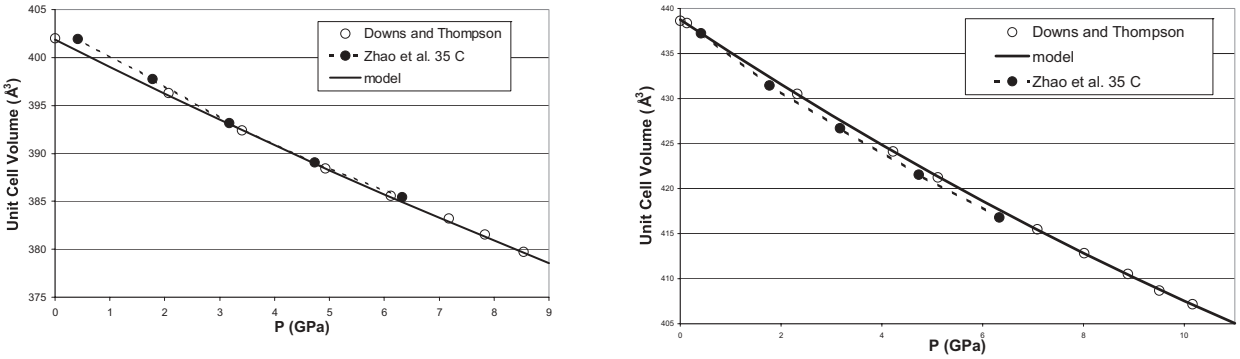

FIGURE 12. A comparison of Zhao et al.'s (1997) 35 °C isotherm for jadeite and diopside with the model derived from Downs and Thompson's (in prep) room *T*, high-*P* data. This shows that there is a systematic error in the model relative to the Zhao et al. (1997) data, because the model was fit to different experimental data. The error is larger for diopside than jadeite.

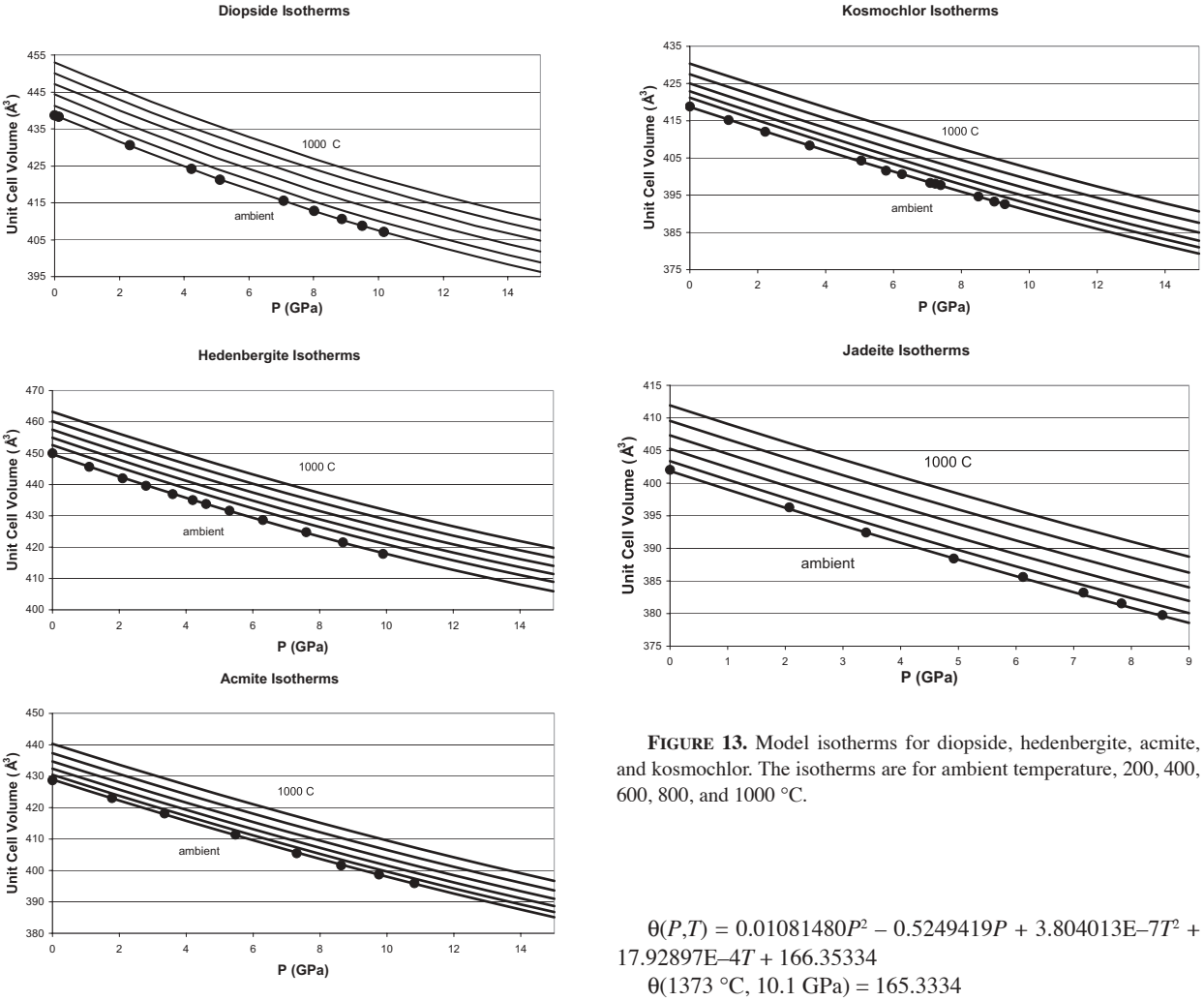

FIGURE 13. Model isotherms for diopside, hedenbergite, acmite, and kosmochlor. The isotherms are for ambient temperature, 200, 400, 600, 800, and 1000 °C.

$\theta(P,T) = a_{\theta P}P^2 + b_{\theta P}P + a_{\theta T}T^2 + a_{\theta T}T + c_{\theta T}$

$r(P,T) = a_{rP}P^2 + b_{rP}P + a_{rT}T^2 + a_{rT}T + c_{rT}$

$V[\theta(P,T), r(P,T)] = (32\sqrt{2}(1 - \cos\theta) + 64(1 - \cos\theta)^{3/2}/\sqrt{3})r^3$.

Obtaining coefficients from Table 5 we obtain for diopside:

$\theta(P,T) = 0.01081480P^2 - 0.5249419P + 3.804013\text{E}{-7}T^2 + 17.92897\text{E}{-4}T + 166.35334$

$\theta(1373\ °C, 10.1\ GPa) = 165.3334$

$r(P,T) = 4.39994\text{E}{-5}P^2 - 3.09581\text{E}{-3}P - 0.976586\text{E}{-9}T^2 + 13.1004\text{E}{-6}T + 1.3177634$

$r(1373\ °C, 10.1\ GPa) = 1.30713$

$V(1373\ °C, 10.1\ GPa) = 426.576\ Å^3$

For hedenbergite:

$\theta(P,T) = 0.01812659P^2 - 0.6480439P - 12.59676\text{E}{-7}T^2 + 42.20255\text{E}{-4}T + 164.3700$

$\theta(1373\ ^\circ\text{C}, 10.1\ \text{GPa}) = 163.0936$

$r(P,T) = 2.24498\text{E}{-5}P^2 - 2.73550\text{E}{-3}P + 4.16204\text{E}{-9}T^2 + 4.71795\text{E}{-6}T + 1.332287$

$r(1373\ ^\circ\text{C}, 10.1\ \text{GPa}) = 1.32127$

$V(1373\ ^\circ\text{C}, 10.1\ \text{GPa}) = 437.555\ \text{Å}^3$

For jadeite:

$\theta(P,T) = 0.006271717P^2 - 0.7020588P + 8.262667\text{E}{-7}T^2 + 3.084192\text{E}{-4}T + 174.5817$

$\theta(1373\ ^\circ\text{C}, 10.1\ \text{GPa}) = 170.1118$

$r(P,T) = 4.14655\text{E}{-5}P^2 - 2.72800\text{E}{-3}P + 1.68733\text{E}{-9}T^2 + 8.62997\text{E}{-6}T + 1.27348$

$r(1373\ ^\circ\text{C}, 10.1\ \text{GPa}) = 1.26519$

$V(1373\ ^\circ\text{C}, 10.1\ \text{GPa}) = 391.241\ \text{Å}^3$.

We linearly combined these volumes to get the volume of the solution:

$V_{soln}(1373\ ^\circ\text{C}, 10.1\ \text{GPa}) = 0.812 \times V_{di}(1373\ ^\circ\text{C}, 10.1\ \text{GPa}) + 0.130 \times V_{hd}(1373\ ^\circ\text{C}, 10.1\ \text{GPa}) + 0.058 \times V_{jd}(1373\ ^\circ\text{C}, 10.1\ \text{GPa}) = 425.95\ \text{Å}^3$.

It is well established (Akimoto et al. 1965; Yamamoto and Akimoto 1977; Pacalo and Gasparik 1990; Kanazaki 1991; Revenaugh and Jordan 1991; Angel et al. 1992; Hugh-Jones et al. 1994; Woodland and Angel 1997; Woodland 1998) that the rock-forming orthopyroxenes transform to *C*2/*c* clinopyroxenes at a depth of approximately 300 km. Therefore, a function that provides volume at *P*, *T*, and *x* for the *C*2/*c* pyroxenes may be useful in modeling deeper portions of the upper mantle.

ACKNOWLEDGMENTS

We thank the M. Tribaudino and an anonymous referee for their time and valuable suggestions. This work was supported with funds provided by the National Science Foundation for the study entitled "Compression of Upper Mantle Minerals," grant No. EAR-9903104.

REFERENCES CITED

Akimoto, S., Katsura, T., Syono, Y., Fujisawa, H., and Komada, E. (1965) Polymorphic transition of pyroxenes $FeSiO_3$ and $CoSiO_3$ at high pressures and temperatures. Journal of Geophysical Research, 70, 5269–5278.

Angel, R.J., Chopelas, A., and Ross, N.L (1992) Stability of high-density clinoenstatite at upper-mantle pressures. Nature, 358, 322–324.

Arlt, T. and Angel, R.J. (2000) Displacive phase transitions in C-centered clinopyroxenes: spodumene, $LiScSi_2O_6$ and $ZnSi_2O_6$. Physics and Chemistry of Minerals, 27, 719–731.

Cameron, M., Sueno, S., Prewitt, C.T., and Papike, J.J. (1973) High-temperature crystal chemistry of acmite, diopside, hedenbergite, jadeite, spodumene, and ureyite. American Mineralogist, 58, 594–618.

Chisholm, J.E. (1981) Pyribole structure types. Mineralogical Magazine, 44, 205–216.

——— (1982) Lowering of symmetry in pyribole structures. Mineralogical Magazine, 45, 25–34.

Deer, W.A., Howie, R.A., and Zussman, J. (1978) Rock-Forming Minerals, Volume 2A, Single Chain Silicates. Wiley, New York.

Dennis Jr., J.E. and Schnabel, R.B. (1983) Numerical Methods for Unconstrained Optimization and Nonlinear Equations. Prentice-Hall, Englewood Cliffs, New Jersey.

Downs, R.T. (2003) Topology of the pyroxenes as a function of temperature, pressure, and composition as determined from the procrystal electron density. American Mineralogist, 88, 556–566.

Duffy, T.S. and Wang, Y. (1998) Pressure-volume-temperature equations of state. In R.J. Hemley, Ed., Ultrahigh-Pressure Mineralogy, Physics and Chemistry of the Earth's Deep Interior. Reviews in Mineralogy and Geochemistry, 37, 425–457. Mineralogical Society of America, Washington, D.C.

Freed, R.L. and Peacor, D.R. (1967) Refinement of the crystal structure of johannsenite. American Mineralogist, 52, 709–720.

Ghose, S., Wan, C., and Okamura, F.P. (1987) Crystal structures of $CaNiSi_2O_6$ and $CaCoSi_2O_6$ and some crystal-chemical relations in *C*2/*c* clinopyroxenes. American Mineralogist, 72, 375–381.

Hattori, T., Nagai, T., Yamanaka, T., Werner, S., and Schulz, H. (2000) Single-crystal X-ray diffraction study of $FeGeO_3$ high-P clinopyroxene (*C*2/*c*) up to 8.2 GPa. American Mineralogist, 85, 1485–1491.

Hawthorne, F.C. and Grundy, H.D. (1977) Refinement of the crystal structure of $LiScSi_2O_6$ and structural variations in alkali pyroxenes. Canadian Mineralogist, 15, 50–58.

Hugh-Jones, D.A., Woodland, A.B., and Angel, R.J. (1994) The structure of high-pressure C2/c ferrosilite and crystal chemistry of high-pressure *C*2/*c* pyroxenes. American Mineralogist, 79, 1032–1041.

Kanazaki, M. (1991) Ortho/clinoenstatite transition. Physics and Chemistry of Minerals, 17, 726–730.

Kopnin, E.M., Sato, A., and Takayama-Muromachi, E. (2003) High pressure synthesis and structure refinement of $LiTiSi_2O_6$. Journal of Alloys and Compounds, 354, L16–L19.

Levien, L. and Prewitt, C.T. (1981) High-pressure structural study of diopside. American Mineralogist, 66, 315–323.

Mao, H. and Hemley, R.J. (1998) New windows on the Earth's deep interior. In R.J. Hemley, Ed., Ultrahigh-pressure Mineralogy, Physics and Chemistry of the Earth's Deep Interior. Reviews in Mineralogy and Geochemistry, 37, 1–32. Mineralogical Society of America, Chantilly, Virginia.

Matsui, M. and Busing, W.R. (1984) Calculation of the elastic constants and high-pressure properties of diopside, $CaMgSi_2O_6$. American Mineralogist, 69, 1090–1095.

Matsui, M. and Price, G.D. (1992) Computer simulation of the $MgSiO_3$ polymorphs. Physics and Chemistry of Minerals, 18, 365–372.

Morimoto, N., Nakajima, Y., Syono, Y., Akimoto, S., and Matsui, Y. (1975) Crystal-structures of pyroxene-type $ZnSiO_3$ and $ZnMgSi_2O_3$. Acta Crystallographica, B31, 1041–1049.

Ohashi, Y. (1984) Polysynthetically-twinned structures of enstatite and wollastonite. Physics and Chemistry of Minerals, 10, 217–229.

Ohashi, H., Fujita, T., and Osawa, T. (1982) The crystal structure of the $NaTiSi_2O_6$ pyroxene. Journal of the Japanese Association of Mineralogists, Petrologists, and Economic Geologists, 77, 305–309.

Ohashi, H., Osawa, T., and Tsukimura, K. (1987) Refinement of the structure of manganese sodium dimetasilicate. Acta Crystallographica, C43, 605–607.

Ohashi, H., Osawa, T., and Sato, A. (1990) Structures of $Na(In,Sc)Si_2O_6$ clinopyroxenes formed at 6-GPa pressure. Acta Crystallographica, B46, 742–747.

——— (1994a) $NaScSi_2O_6$. Acta Crystallographica, C50, 838–840.

——— (1994b) $NaVSi_2O_6$. Acta Crystallographica, C50, 1652–1655.

——— (1995) Low density form of $NaGaSi_2O_6$. Acta Crystallographica, C51, 2476–2477.

——— (2003a) Crystal structures of $Ca(Mn,Zn)Si_2O_6$ clinopyroxenes formed at 6 GPa. In H. Ohashi, Ed., X-Ray Study on Si-O Bonding, 1–21. Haruo Ohashi, Maruzen Publishing Service Center, Tokyo, Japan.

——— (2003b) Electron density effect on Si-O2 distance in $Na(In,Sc)Si_2O_6$ clinopyroxenes. In H. Ohashi, Ed., X-Ray Study on Si-O Bonding, 29–40. Haruo Ohashi, Maruzen Publishing Service Center, Tokyo, Japan.

——— (2003c) Crystal structures of $(Na,Ca)(Ti,Mg)Si_2O_6$ pyroxenes. In H. Ohashi, Ed., X-Ray Study on Si-O Bonding, 41–58. Haruo Ohashi, Maruzen Publishing Service Center, Tokyo, Japan.

——— (2003d) Crystal structures of $(Na,Ca)(V,Mn)Si_2O_6$ pyroxenes. In H. Ohashi, Ed., X-Ray Study on Si-O Bonding, 59–71. Haruo Ohashi, Maruzen Publishing Service Center, Tokyo, Japan.

——— (2003e) Crystal structures of $(Na,Ca)(V,Mg)Si_2O_6$ pyroxenes. In H. Ohashi, Ed., X-Ray Study on Si-O Bonding, 72–82. Haruo Ohashi, Maruzen Publishing Service Center, Tokyo, Japan.

——— (2003f) Discontinuous changes of chromium electronegativity in $(Na,Ca)(Cr,Mg)Si_2O_6$ clinopyroxenes. In H. Ohashi, Ed., X-Ray Study on Si-O Bonding, 91–98. Haruo Ohashi, Maruzen Publishing Service Center, Tokyo, Japan.

——— (2003g) Crystal structure variations of $(Na,Ca)(Cr,Mg)Si_2O_6$ pyroxenes reflecting synthetic conditions. In H. Ohashi, Ed., X-Ray Study on Si-O Bonding, 99–108. Haruo Ohashi, Maruzen Publishing Service Center, Tokyo, Japan.

——— (2003h) Transitional structures of $Na(Ga,Al)Si_2O_6$ clinopyroxenes formed at 6 GPa pressure. In H. Ohashi, Ed., X-Ray Study on Si-O Bonding, 114–133. Haruo Ohashi, Maruzen Publishing Service Center, Tokyo, Japan.

——— (2003i) Crystal structures of $Na(Ga,Sc)Si_2O_6$ clinopyroxenes formed at 6 GPa pressure. In H. Ohashi, Ed., X-Ray Study on Si-O Bonding, 134–145. Haruo Ohashi, Maruzen Publishing Service Center, Tokyo, Japan.

——— (2003j) Crystal structures of $Li(Al,Ga)Si_2O_6$ pyroxenes. In H. Ohashi, Ed., X-Ray Study on Si-O Bonding, 146–158. Haruo Ohashi, Maruzen Publishing Service Center, Tokyo, Japan.

Okamura, F.P., Ghose, S., and Ohashi, H. (1974) Structure and crystal chemistry

of calcium Tshermak's pyroxene, $CaAlAlSiO_6$. American Mineralogist, 59, 549–557.
Olkin, I., Gleser, L.J., and Derman, C. (1980) Probability Models and Applications. Macmillan Publishing Co., Inc., New York.
Origlieri, M., Downs, R.T., Thompson, R.M., Pommier, C.J.S., Denton, M.B., and Harlow, G.E. (2003) High-pressure crystal structure of kosmochlor, $NaCrSi_2O_6$ and systematics of anisotropic compression of pyroxenes. American Mineralogist, 88, 1025–1032.
Pacalo, R.E.G. and Gasparik, T. (1990) Reversals of the orthoenstatite-clinoenstatite transition at high pressures and high temperatures. Journal of Geophysical Research, 95, 15853–15858.
Pannhorst, W. (1979) Structural relationships between pyroxenes. Neues Jahrbuch für Mineralogie-Abhandlungen, 135, 1–17.
——— (1981) Comparison between topological classifications of pyroxenes. Neues Jahrbuch für Mineralogie-Abhandlungen, 143, 1–14.
Papike, J.J., Prewitt, C.T., Sueno, S., and Cameron, M. (1973) Pyroxenes: comparisons of real and ideal structural topologies. Zeitschrift für Kristallographie, 138, 254–273.
Raudsepp, M., Hawthorne, F.C., and Turnock, A.C. (1990a) Evaluation of the Rietveld method for the characterization of fine-grained products of mineral synthesis: the diopside-hedenbergite join. Canadian Mineralogist, 28, 93–109.
——— (1990b) Crystal chemistry of synthetic pyroxenes on the join $CaNiSi_2O_6$–$CaMgSi_2O_6$ (diopside): a Rietveld structure refinement study. American Mineralogist, 75, 1274–1281.
Redhammer, G.J. and Roth, G. (2004) Structural variation and crystal chemistry of $LiMe^{3+}Si_2O_6$ clinopyroxenes Me^{3+} = Al, Ga, Cr, V, Fe, Sc, In. Zeitschrift für Kristallographie, 219, 278–294.
Redhammer, G.J., Amthauer, G., Lottermoser, W., and Treutmann, W. (2000) Synthesis and structural properties of clinopyroxenes of the hedenbergite $CaFeSi_2O_6$—aegerine $NaFe^{3+}Si_2O_6$ solid-solution series. European Journal of Mineralogy, 12, 105–120.
Redhammer, G.J., Roth, G., Paulus, W., André, G., Lottermoser, W., Amthauer, G., Treutmann, W., and Koppelhuber-Bitschnau, B. (2001) The crystal and magnetic structure of Li-aegerine $LiFe^{3+}Si_2O_6$: a temperature-dependent study. Physics and Chemistry of Minerals, 28, 337–346.
Redhammer, G.J., Ohashi, H., and Roth, G. (2003) Single-crystal structure refinement of $NaTiSi_2O_6$ clinopyroxene at low temperatures ($298 < T < 100$ K). Acta Crystallographica, B59, 730–746.
Revenaugh, J. and Jordan, T.H. (1991) Mantle layering from ScS reverberations 3. The upper mantle. Journal of Geophysical Research, 96, 19781–19810.
Robinson, K., Gibbs, G.V., and Ribbe, P.H. (1971) Quadratic elongation: a quantitative measure of distortion in coordination polyhedra. Science, 172, 567–570.
Sato, A., Osawa, T., and Ohashi, H. (1994) $LiGaSi_2O_6$. Acta Crystallographica, C50, 487–488.
Satto, C., Millet, P., and Galy, J. (1997) Lithium vanadium metasilicate, $LiVSi_2O_6$. Acta Crystallographica, C53, 1727–1728.
Shannon, R.D. (1976) Revised effective ionic radii and systematic studies of interatomic distances in halides and chalcogenides. Acta Crystallographica, A32, 751–767.
Thompson, J.B. (1970) Geometrical possibilities for amphibole structures: model biopyriboles. American Mineralogist, 55, 292–293.
Thompson, R.M. (2004) Crystallographic model of the pyroxenes. Ph.D. dissertation, University of Arizona. UMI Dissertation Services.
Thompson, R.M. and Downs, R.T. (2003) Model pyroxenes I: Ideal pyroxene topologies. American Mineralogist, 88, 653–666.
——— (2004) Model pyroxenes II: Structural variation as a function of tetrahedral rotation. American Mineralogist, 89, 614–628.
Tribaudino, M. (1996) High-temperature crystal chemistry of *C*2/*c* clinopyroxenes along the join $CaMgSi_2O_6$–$CaAl_2SiO_6$. European Journal of Mineralogy, 8, 273–279.
——— (2000) A transmission electron microscope investigation of the *C*2/*c* → $P2_1/c$ phase transition in clinopyroxenes along the diopside-enstatite ($CaMgSi_2O_6$–$Mg_2Si_2O_6$) join. American Mineralogist, 85, 707–715.
Tribaudino, M., Prencipe, M., Bruno, M., and Levy, D. (2000) High-pressure behaviour of Ca-rich *C*2/*c* clinopyroxenes along the join diopside–enstatite ($CaMgSi_2O_6$–$Mg_2Si_2O_6$). Physics and Chemistry of Minerals, 27, 656–664.
Tribaudino, M., Prencipe, M., Nestola, F., and Hanfland, M. (2001) A $P2_1/c$–*C*2/*c* high-pressure phase transition in $Ca_{0.5}Mg_{1.5}Si_2O_6$ clinopyroxene. American Mineralogist, 86, 807–813.
Tribaudino, M., Nestola, F., Cámara, F., and Domeneghetti, M.C. (2002) The high-temperature $P2_1/c$–*C*2/*c* phase transition in Fe-free pyroxene ($Ca_{0.15}Mg_{1.85}Si_2O_6$): structural and thermodynamic behavior. American Mineralogist, 87, 648–657.
Wood, B.J., Holland, T.J.B., Newton, R.C., and Kleppa, O.J. (1980) Thermochemistry of jadeite–diopside pyroxenes. Geochimica et Cosmochimica Acta, 44, 1363–1371.
Woodland, A.B. (1998) The orthorhombic to high-P monoclinic phase transition in Mg-Fe pyroxenes: Can it produce a seismic discontinuity? Geophysical Research Letters, 25, 1241–1244.
Woodland, A.B. and Angel, R.J. (1997) Reversal of the orthoferrosilite – high-P clinoferrosilite transition, a phase diagram for $FeSiO_3$ and implications for the mineralogy of the Earth's upper mantle. European Journal of Mineralogy, 9, 245–254.
Yamamoto, K. and Akimoto, S. (1977) The system MgO-SiO_2-H_2O at high pressures and temperatures: stability field for hydroxyl-chondrodite, hydroxyl-clinohumite and 10Å phase. American Journal of Science, 277, 288–312.
Zhang, L., Ahsbahs, H., Hafner, S., and Kutoglu, A. (1997) Single-crystal compression and crystal structure of clinopyroxene up to 10 GPa. American Mineralogist, 82, 245–258.
Zhao, Y., Von Dreele, R.B., Shankland, T.J., Weidner, D.J., Zhang, J., Wang, Y., and Gasparik, T. (1997) Thermoelastic equation of state of jadeite $NaAlSi_2O_6$: an energy-dispersive Reitveld refinement study of low symmetry and multiple phases diffraction. Geophysical Research Letters, 24, 5–8.
Zhao, Y., Von Dreele, R.B., Zhang, J., and Weidner, D.J. (1998) Thermoelastic equation of state of monoclinic pyroxene: $CaMgSi_2O_6$ diopside. The Review of High Pressure Science and Technology, 7, 25–27.

MANUSCRIPT RECEIVED NOVEMBER 18, 2004
MANUSCRIPT ACCEPTED APRIL 4, 2005
MANUSCRIPT HANDLED BY GEORGE LAGER